of the asymmetric unit, there was significant correlation in the least-squares refinement, and damping was required for initial stages of refinement.

2-Ni: Red plates were obtained from vapor diffusion of $ClCH_2CH_2Cl$ into a CH_3NO_2 solution. CH_3NO_2 was found in the difference Fourier map; anisotropic refinement was successful. Large thermal anisotropy was evident in the counterions, but was not further modeled.

3-Ni: Large red prisms were grown by vapor diffusion of $ClCH_2CH_2Cl$ into a CH_3NO_2 solution. A difference peak was ascribed to $ClCH_2CH_2Cl$; the solvent molecule resides on an inversion center and was successfully refined with anisotropic thermal motion. Much disorder, interpreted as rotation about a Cl-O bond of a perchlorate anion, was evident; the remaining three oxygens were refined as disordered pairs, each with half occupancy and isotropic thermal motion constrained to 0.03. Residual electron density was near the perchlorate.

Acknowledgment. S.H.G. thanks the Searle Scholars Program and the American Cancer Society (Junior Faculty Research Award) for partial support. J.M.D. thanks the Graduate School of the University of Wisconsin—Madison for a fellowship. S.R.C. acknowledges support from the Petroleum Research Fund, administered by the American Chemical Society. S.H.G. thanks Tim Clark (Visiting Professor of Chemistry, University of Wisconsin—Madison, Spring 1991) for helpful discussions on computational issues.

Spectroscopic and Theoretical Studies of an End-On Peroxide-Bridged Coupled Binuclear Copper(II) Model Complex of Relevance to the Active Sites in Hemocyanin and Tyrosinase

Michael J. Baldwin,[†] Paul K. Ross,[†] James E. Pate,[†,‡] Zoltán Tyeklár,[§] Kenneth D. Karlin,[§] and Edward I. Solomon*,[†]

Contribution from the Department of Chemistry, Stanford University, Stanford, California 94305, Department of Chemistry, The Johns Hopkins University, Baltimore, Maryland 21218, and Dow Chemical Company, Central Research, Advanced Polymeric Systems Laboratory, Midland, Michigan 48674. *Received April 25, 1991*

Abstract: Spectroscopic studies have been combined with broken-symmetry SCF-Xα-SW calculations to determine the vibrational and electronic structure of peroxide–copper bonding in the end-on trans μ-1,2 peroxide-bridged copper dimer, $[\{Cu(TMPA)\}_2(O_2)]^{2+}$. This study provides a detailed understanding of the electronic structure generally associated with an end-on peroxide-bridging mode and additionally shows important dimer interactions which are not present in the copper–peroxide monomer. The Xα calculations show that the electronic structure is dominated by the interaction of the peroxide π^*_σ orbital with the half-occupied copper d_{z^2} orbitals. This copper–peroxide bonding is probed experimentally by a peroxide-to-copper charge-transfer spectrum which contains three transitions at 615 (ϵ = 5800 M^{-1} cm^{-1}), 524 (ϵ = 11 300 M^{-1} cm^{-1}), and 435 nm (ϵ = 1700 M^{-1} cm^{-1}) assigned as the electric dipole allowed singlet transitions from π^*_v and π^*_σ (the HOMO orbitals of peroxide) and the spin-forbidden triplet from π^*_v, respectively. The differences between the observed and calculated transition energies, which are present in the dimer but not the monomer, are shown to arise from excited-state splittings which derive from excitation transfer in the dimer and from excited-state exchange interactions much larger than those in the dimer ground state [$-2J_{es}(\pi^*_v) \approx 7600$ cm^{-1}]. The resonance Raman spectra show two enhanced vibrations which shift upon isotopic substitution of $^{16}O_2$ by $^{18}O_2$ at 832 (788 cm^{-1} with $^{18}O_2$) and 561 cm^{-1} (535 cm^{-1} with $^{18}O_2$). They are assigned as the intraperoxide stretch and the symmetric copper–oxygen stretch, respectively. A normal-coordinate analysis has been performed using these vibrational data to compare this trans μ-1,2 dimer to a previously studied monomer. This analysis shows that the O–O bond force constant, k_{O-O}, increases upon going from the monomer to the dimer due to increased donation of electron density from the antibonding π^*_σ orbital to the second copper in the dimer. The resonance enhancement of the intraperoxide stretch is similar to that of the monomer; however, the enhancement behavior of the copper–oxygen stretch is significantly different from that in the monomer, showing enhancement only from the π^*_v transitions. This enhancement behavior is discussed with respect to excited-state distortions of the dimer which can be very different from the monomer depending on the extent of delocalization (i.e. electron coupling) of the charge-transfer excitation over the two halves of the dimer.

Introduction

The electronic, vibrational, and chemical properties of copper–peroxide bonding have long been of interest due to the importance of copper–peroxide complexes in reversible oxygen binding and oxidation and oxygenation catalysis, especially in such biological systems as hemocyanin,[1] tyrosinase,[2] and the multicopper oxidases.[3] Several different binding modes of peroxide to copper(II) are known. An end-on bound monomer[4] (structure A in Scheme I), $[Cu_2(XYL-O-)(O_2)]^+$, was studied previously in solution but could not be crystallized. Complexes with a binding mode like that of structure B in Scheme I are also known,[5] and a μ-1,1 acylperoxo complex of this type has been structurally characterized.[6] While the cis μ-1,2 structure C of Scheme I is

* Author to whom correspondence should be directed.
† Stanford University.
§ Johns Hopkins University.
‡ Dow Chemical Company.

(1) (a) Solomon, E. I.; Penfield, K. W.; Wilcox, D. E. *Structure and Bonding (Berlin)* **1983**, *53*, 1-57. (b) Solomon, E. I. *Pure Appl. Chem.* **1983**, *55*, 1069-1088. (c) Solomon, E. I. In *Copper Proteins*; Spiro, T. G., Ed.; Wiley: New York, 1981; pp 41-108.

(2) Lerch, K. *Metal Ions Biol. Syst.* **1981**, *13*, 143-186.

(3) (a) Cole, J. L.; Tan, G. O.; Yang, E. K.; Hodgson, K. O.; Solomon, E. I. *J. Am. Chem. Soc.* **1990**, *112*, 2243-2249. (b) Andreasson, L. E.; Branden, R.; Reinhammer, B. *Biochim. Biophys. Acta* **1976**, *438*, 370-379.

(4) (a) Pate, J. E.; Cruse, R. W.; Karlin, K. D.; Solomon, E. I. *J. Am. Chem. Soc.* **1987**, *109*, 2624-2630. (b) In this paper the term "monomer" refers to peroxide bound to a single copper ion; the term "dimer" refers to peroxide bridging a pair of copper ions and mediating interactions between those copper ions.

(5) Karlin, K. D.; Cruse, R. W.; Gultneh, Y. *J. Chem. Soc., Chem. Commun.* **1987**, 599-600.

0002-7863/91/1513-8671$02.50/0

Scheme I

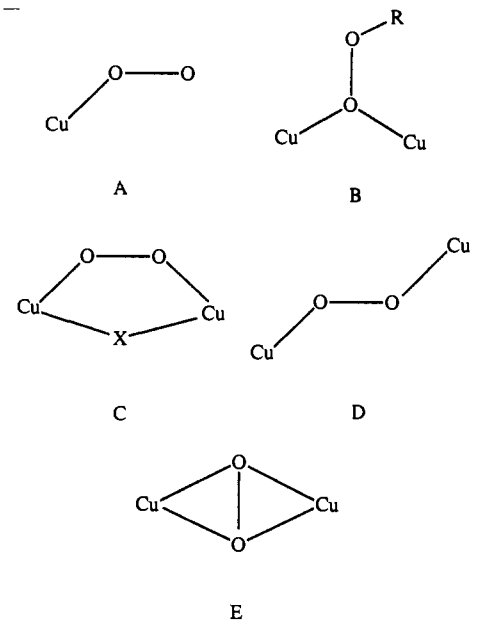

quite common for cobalt(III) dimers (X = OH^-, NH_2^-),[7] no complex with this structure is yet established for copper. This study concerns the structurally characterized complex $[\{Cu(TMPA)\}_2(O_2)](PF_6)_2$ (TMPA = tris(2-methylpyridyl)amine), which has the trans μ-1,2 binding mode corresponding to structure D in Scheme I.[8] A complex with a μ-η^2:η^2 binding mode as in structure E of Scheme I has also been characterized by X-ray crystallography.[9] Calculations by Ross and Solomon[10] have shown that while the electronic structures of the two end-on μ-1,2 dimers, C and D in Scheme I, are qualitatively similar, the side-on μ-η^2:η^2 binding mode of structure E is fundamentally different. This study of the end-on bridged trans μ-1,2 copper–peroxide dimer, $[\{Cu(TMPA)\}_2(O_2)](PF_6)_2$, provides a detailed understanding of the electronic structure generally associated with an end-on peroxide-binding mode and additionally shows important dimer interactions which are absent in the copper–peroxide monomer.

The highest occupied molecular orbitals of free peroxide ion are a doubly degenerate set of antibonding π^* orbitals which play the key role in its bonding to copper(II). Upon binding, the degeneracy of this π^* pair is removed by unequal interactions with the metal d orbitals which act as the acceptor orbitals in forming the metal–peroxide bond. The peroxide π^* orbital which has greatest overlap with the metal-based acceptor orbital through a σ-bonding interaction is designated as π^*_σ, and the orbital which is vertical to the metal–peroxide plane is designated as π^*_v. In a monomeric copper(II)–peroxide complex, two $O_2^{2-}(\pi^*) \rightarrow$ Cu(II) charge-transfer transitions from the π^*_v and π^*_σ orbitals to the half-filled d orbital on the copper are expected. Due to greater overlap, the transition from π^*_σ is expected to exhibit greater absorption intensity and be observed at higher energy than the transition from π^*_v. In our previous spectroscopic investigation of the end-on bound copper–peroxide monomer $[Cu_2(XYL\text{-}O\text{-})(O_2)]^+$, a charge-transfer absorption spectrum entirely consistent with this description was observed.[4a] Two intense bands in the visible absorption spectrum are assigned as peroxide-to-copper charge-transfer transitions. The higher energy band at 503 nm (19900 cm^{-1}, ϵ = 5800 M^{-1} cm^{-1}), assigned as $\pi^*_\sigma \rightarrow Cu(d_{x^2-y^2})$, is significantly more intense than the lower energy band at 625 nm (16000 cm^{-1}, ϵ = 1100 M^{-1} cm^{-1}), assigned as $\pi^*_v \rightarrow Cu(d_{x^2-y^2})$. Two peaks are present in the resonance Raman spectra of this complex.[4] One peak, at 803 cm^{-1}, identified as the intraperoxide stretching frequency, showed resonance enhancement from both of the $O_2^{2-}(\pi^*) \rightarrow$ Cu(II) CT transitions, but with relatively greater enhancement from the π^*_v transition. The second feature, seen at 488 cm^{-1} and identified as the copper–oxygen stretching frequency, showed greater enhancement from the π^*_σ transition.

The end-on peroxide-bridged copper dimer $[\{Cu(TMPA)\}_2(O_2)](PF_6)_2$ has been characterized by X-ray crystallography.[8] The complex contains two Cu(II) ions with distorted trigonal-bipyramidal ligand fields bridged by peroxide in a trans μ-1,2 configuration (structure D in Scheme I). The other ligands are three pyridyl nitrogens in the equatorial positions of each copper and a saturated amine in the axial position opposite the peroxide. The overall point group symmetry of the dimer is C_i, while the planar Cu_2O_2 unit has C_{2h} symmetry. The dimer shows strong antiferromagnetic coupling, with a singlet–triplet splitting, $-2J > 600$ cm^{-1}.[11] The visible absorption spectrum shows several intense features which are absent in $[Cu(TMPA)Cl]^+$, a chloride analogue of the peroxide-bridged complex with a similar ligand geometry around the copper.[12] In this paper, we present vibrational, resonance Raman, and electronic absorption studies of $[\{Cu(TMPA)\}_2(O_2)](PF_6)_2$ as well as broken-symmetry self-consistent-field Xα scattered-wave (SCF-Xα-SW) calculations[13] on an idealized $[(NH_3)_4CuO_2Cu(NH_3)_4]^{2+}$ structure. These studies allow a detailed analysis of the vibrational structure of the end-on peroxide-bridged binuclear copper site, of the electronic structure of the ground and excited states of the end-on bridged dimer, and of the nuclear distortions which occur upon transition to these excited states. In addition to a description of end-on peroxide–copper bonding, these studies show important effects on the vibrational and electronic structure upon going from a monomer to a bridged dimer. Dimer interactions in weakly coupled ligand-field excited states have been thoroughly studied in copper acetate,[14] and dimer interactions have been invoked to explain the excited-state splitting observed for a charge-transfer excited state in azide-bridged copper(II) dimers.[15] In this study we find important dimer effects on the excited-state energy splittings as well as on the excited-state distortions of the peroxide-to-copper charge-transfer states.

Experimental Section

The purple $[\{Cu(TMPA)\}_2(O_2)](PF_6)_2$[8] and blue $[Cu(TMPA)Cl](PF_6)$[12] were prepared as previously described. The isotope-substituted material was prepared using 98% $^{18}O_2$ (ICON Services; Summit, NJ). The UV/vis spectrum of the peroxide complex was taken in propionitrile at −85 °C on a Perkin-Elmer 3840 spectrophotometer. The near-IR spectrum was taken on a Shimadzu UV-160 spectrophotometer. The UV/vis and near-IR absorption spectra of $[Cu(TMPA)Cl](PF_6)$ were taken in propionitrile at room temperature on a Cary 17 spectrophotometer which is interfaced to a Compaq 386 computer. The sample for the mull spectrum of $[\{Cu(TMPA)\}_2(O_2)](PF_6)_2$ was prepared in a glovebag filled with dry nitrogen gas by grinding the powder in a mortar embedded

(6) Ghosh, P.; Tyeklär, Z.; Farooq, A.; Karlin, K. D.; Jacobson, R. R.; Zubieta, J. *J. Am. Chem. Soc.* **1987**, *109*, 6889–6891.
(7) (a) Jones, R. D.; Summerville, D. A.; Basolo, F. *Chem. Rev.* **1979**, *79*, 139–179. (b) Niederhoffer, E. C.; Timmons, J. H.; Martell, A. E. *Chem. Rev.* **1984**, *84*, 137–203.
(8) Jacobson, R. R.; Tyeklär, Z.; Farooq, A.; Karlin, K. D.; Liu, S.; Zubieta, J. *J. Am. Chem. Soc.* **1988**, *110*, 3690–3692.
(9) Kitajima, N.; Fujisawa, K.; Moro-oka, Y. *J. Am. Chem. Soc.* **1989**, *111*, 8975–8976.
(10) (a) Ross, P. K.; Solomon, E. I. *J. Am. Chem. Soc.* **1990**, *112*, 5871–5872. (b) Ross, P. K.; Solomon, E. I. *J. Am. Chem. Soc.* **1991**, *113*, 3246–3259.
(11) Karlin, K. D.; Tyeklär, Z.; Farooq, A.; Jacobson, R. R.; Sinn, E.; Lee, D. W.; Bradshaw, J. E.; Wilson, L. J. *Inorg. Chim. Acta* **1991**, *182*, 1–3.
(12) Karlin, K. D.; Hayes, J. C.; Juen, S.; Hutchinson, J. P.; Zubieta, J. *Inorg. Chem.* **1982**, *21*, 4106–4108.
(13) (a) Slater, J. C. *Adv. Quantum Chem.* **1972**, *6*, 1–92. (b) Johnson, K. H. *Adv. Quantum Chem.* **1973**, *7*, 143–185. (c) Case, D. A. *Annu. Rev. Phys. Chem.* **1982**, *33*, 151–171. (d) Johnson, K. H. *Annu. Rev. Phys. Chem.* **1975**, *26*, 39–42. (e) Connolly, J. W. D. In *Semiempirical Methods of Electronic Structure Calculation, Part A: Techniques*; Segal, G. A., Ed.; Plenum: New York, 1977; pp 105–132. (f) Johnson, K. H.; Norman, J. G., Jr.; Connolly, J. W. D. In *Computational Methods for Large Molecules and Localized States in Solids*; Herman, F., McLean, A. D., Nesbet, R. K., Eds.; Plenum: New York, 1973; pp 161–201. (g) Cook, M. R., Ph.D. Thesis, Harvard University, 1981.
(14) Ross, P. K.; Allendorf, M. D.; Solomon, E. I. *J. Am. Chem. Soc.* **1989**, *111*, 4009–4021.
(15) Pate, J. E.; Ross, P. K.; Thamman, T. J.; Reed, C. A.; Karlin, K. D.; Sorrell, T. N.; Solomon, E. I. *J. Am. Chem. Soc.* **1989**, *111*, 5198–5209.

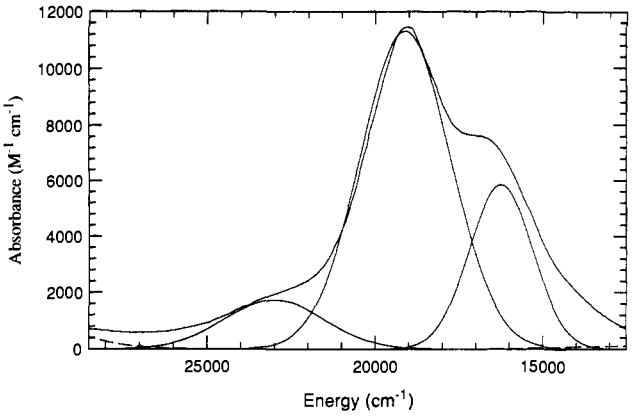

Figure 1. Optical absorption spectrum in the charge-transfer transition region of $[\{Cu(TMPA)\}_2(O_2)](PF_6)_2$ at −85 °C (solid line, with Gaussian resolution shown) and the chloride analogue $[Cu(TMPA)Cl](PF_6)$ at room temperature (dashed line, low absorbance). Both are in propionitrile solution.

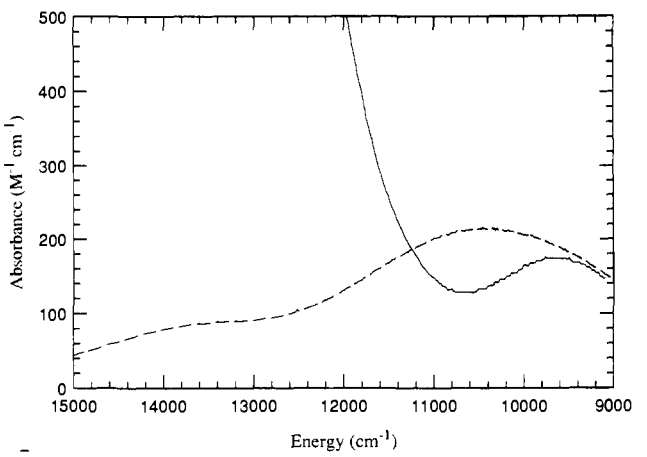

Figure 2. Optical absorption spectrum in the ligand field transition region of $[\{Cu(TMPA)\}_2(O_2)](PF_6)_2$ at −85 °C (solid line) and $[Cu(TMPA)Cl](PF_6)$ at room temperature (dashed line). Both are in propionitrile solution.

in dry ice and mulling with toluene. The mull was spread between two infrasil quartz disks, placed in a copper holder, and immediately immersed in liquid nitrogen. The mull spectrum was taken on a McPherson RS-10 double-beam spectrophotometer with a Janis Vari-Temp helium Dewar.

Resonance Raman samples were prepared by grinding the solid material either by itself or with an appropriate amount of KBr or, when an internal standard was used for enhancement profiles, K_2SO_4 in a mortar embedded in dry ice. The homogeneously mixed solid samples were then put into 1 mm i.d. capillary tubes and kept on dry ice. Resonance Raman spectra were measured using a Spex 1403 double monochromator with a cooled RCA C31034A photomultiplier combined with a Spex digital photometer system. This spectrometer is interfaced to a Compaq 286 computer using a program written in our laboratory for driving the monochromator and collecting and analyzing the data. Light sources include a Coherent I-18UV argon ion laser, a Coherent I-90K Krypton ion laser, and Rhodamine 6G and Stilbene 3 dye lasers. The samples were cooled using a nitrogen flow system which allows liquid nitrogen cooled gas to flow over the sample, keeping it at about 110 K. An approximately 180° backscattering geometry was used to collect scattered light from the sample. Laser power was typically 50 mW. The 984-cm^{-1} Raman peak of solid K_2SO_4 was used for intensity calibration of the 832-cm^{-1} peak in the peroxide complex, and all other peak intensities were compared to the 832-cm^{-1} peak for enhancement profiles. Depolarization ratios were determined from propionitrile solutions of the complex using the same experimental setup as for the solid samples, except that a 90° scattering geometry was employed and the nitrogen flow was cooled by a dry ice/acetone bath to prevent the sample from freezing.

The normal coordinate analysis was based on a Wilson FG matrix method[16] using a modified Urey–Bradley force field. The calculations were performed on an IBM PC computer using a modified Schachtschneider program.[17]

Spin-unrestricted, broken-symmetry SCF-Xα-SW calculations[13] were performed on $[(NH_3)_4CuO_2Cu(NH_3)_4]^{2+}$ following procedures described elsewhere.[10] The geometry is based on average values of bond lengths and angles in the reported crystal structure[8] idealized to trigonal-bipyramidal coordination about each copper and a C_{2h} total molecular symmetry. The position of the atoms and α values[18] used in the calculations are given in the supplementary material (Table S1). As with previous Xα calculations on copper–peroxide complexes,[10] all calculations were performed with three sets of atomic sphere radii, with all radii based on the Norman criteria[19] except for copper. Copper sphere radii of 2.33 (the Norman value), 2.60, and 2.95 bohr were used. The energies and charge distributions for the one-electron eigenfunctions for all three sets of radii are given in the supplementary material (Table S2).

Results

The absorption spectrum of $[\{Cu(TMPA)_2\}(O_2)]^{2+}$ taken in propionitrile at −85 °C, shown in Figure 1, has an intense feature with a maximum at 525 nm (19 050 cm^{-1}), an intense shoulder to lower energy, and a weaker shoulder to higher energy. A low-temperature (8 K) mull spectrum was taken to confirm that the complex in solution is the same as the solid. It contained a significant contribution on the low-energy side due to the thermal decomposition products produced during preparation of the mull sample, however, all three of the features observed in the solution spectrum were also observed in the mull spectrum with energies and relative intensities close to those of the solution spectrum. A Gaussian resolution of the solution absorption spectrum in Figure 1 reveals three distinct bands.[20] The most intense band is centered at 524 nm (19 100 cm^{-1}, ϵ = 11 300 M^{-1} cm^{-1}), with the others at 615 (16 250 cm^{-1}, ϵ = 5800 M^{-1} cm^{-1}) and 435 nm (23 000 cm^{-1}, ϵ = 1700 M^{-1} cm^{-1}). There is additional intensity on the low-energy side of the 615-nm band, at approximately the same energy as the contribution from the decomposition products in the mull. An additional weaker band is observed at 1035 nm (9660 cm^{-1}, ϵ = 180 M^{-1} cm^{-1}) in Figure 2. In comparison, $[Cu(TMPA)Cl]^+$ has a weak band at 952 nm (10 500 cm^{-1}, ϵ = 200 M^{-1} cm^{-1}) with a shoulder at ~760 nm (13 200 cm^{-1}, ϵ = 80 M^{-1} cm^{-1}), and no other features at wavelengths greater than 300 nm.

The resonance Raman spectra between 200 and 1000 cm^{-1} of $[\{Cu(TMPA)\}_2(O_2)]^{2+}$ as a powder,[21] taken with excitation energies near resonance with each visible absorption band, are presented in Figure 3. These spectra show a strong peak at 832 cm^{-1} (molar scattering intensity ~10^2× that of $\nu_1(K_2SO_4)$ at 5682 Å), a less intense peak at 561 cm^{-1}, and relatively weak peaks at 650, 430, 333, 255, and 225 cm^{-1}. As shown on the right side of Figure 4, isotopic substitution with $^{18}O_2$ shifts the peak at 832 cm^{-1} to 788 cm^{-1}, and the 561-cm^{-1} peak shifts to 535 cm^{-1}. None of the peaks below 500 cm^{-1}, shown on the left side of Figure 4, nor the 650-cm^{-1} peak on the right side of Figure 4, shift upon isotopic perturbation. In propionitrile solution at 190 K, the 832- and 561-cm^{-1} peaks shift to 826 and 554 cm^{-1}, respectively, and each has a depolarization ratio of 0.4 with 5682-Å excitation.

All of the observed Raman peaks show resonance enhancement from one or more of the absorption bands in the visible region.

(16) (a) McIntosh, D. F.; Michaelian, K. H. *Can. J. Spectrosc.* **1979**, *24*, 1–10. (b) McIntosh, D. F.; Michaelian, K. H. *Ibid.* **1979**, *24*, 35–40. (c) McIntosh, D. F.; Michaelian, K. H. *Ibid.* **1979**, *24*, 65–74.

(17) (a) Schachtschneider, J. H. Technical Report No. 57-65, Shell Development Co., Emeryville, CA, 1966. (b) Fuhrer, H.; Kartha, V. B.; Kidd, K. G.; Kreuger, P. J.; Mantsch, H. H. Computer Programs for Infrared Spectroscopy, Bulletin No. 15, National Research Council of Canada, 1976.

(18) (a) Schwartz, K. *Phys. Rev. B* **1972**, *5*, 2466–2468. (b) Schwartz, K. *Theor. Chim. Acta* **1974**, *34*, 225–231.

(19) (a) Norman, J. G., Jr. *J. Chem. Phys.* **1974**, *61*, 4630–4635. (b) Norman, J. G., Jr. *Mol. Phys.* **1976**, *31*, 1191–1198.

(20) Equally good fits may be obtained by significantly varying the intensities and bandwidths of the Gaussians; however, the positions of the Gaussian maxima vary by only several hundred wavenumbers. The Gaussian fit with the greatest intensity of the center band is shown in Figure 1.

(21) Resonance Raman spectra were taken on the pure powder or on the powder dispersed in powdered KBr, or when an internal standard was used it was dispersed in powdered K_2SO_4. The peak positions reported in the text are for the pure powder and the powder in KBr, which give identical peak positions. In K_2SO_4, the peak positions increase by about 2 cm^{-1}.

Table I. Normal Coordinate Analysis of an End-On Copper–Peroxide Monomer and Dimer

	vibrational frequencies, cm^{-1}						
	experimental		calc(monomer fc's)[a]		calc(dimer fc's)[b]		calc fc,[c]
normal mode	$^{16}O_2$	$^{18}O_2$	$^{16}O_2$	$^{18}O_2$	$^{16}O_2$	$^{18}O_2$	mdyn/Å
monomer							
ν(O–O)	803	750	799.1	753.5			2.929
ν(Cu–O)	488	465	487.9	465.2			1.773
δ(Cu–O–O)	*174*[d]	*170*[d]	173.6	165.7			0.240
trans dimer							
ν(O–O)	832	788	808.7	762.6	833.7	786.2	3.103
ν_s(Cu–O)	561	535	519.4	493.6	561.4	533.1	1.942
ν_{as}(Cu–O)			491.1	468.8	513.5	490.1	
δ_s(Cu–O–O)	*140*[e]		124.5	123.7	139.8	139.0	0.346
δ_{as}(Cu–O–O)			108.3	103.4	125.9	120.2	

[a] Vibrational frequencies calculated from the force constants derived for the monomer structure. [b] Vibrational frequencies calculated from the force constants derived for the trans dimer structure. [c] Force constants derived from the fit of vibrational frequencies to the monomer (top) or dimer (bottom) complex. [d] Symmetric bending frequency taken from the cobalt complex in ref 25 as described in the text. [e] Symmetric bending frequency chosen as described in the text.

The profiles in Figure 5 show strong enhancement of the 832-cm^{-1} peak from the 615-nm band, and weaker enhancement from the more intense 524-nm band. It appears to be enhanced by the 435-nm band as well, although overlap of this feature with the 524-nm band makes this unclear. Figure 5 shows strikingly different resonance enhancement behavior for the 561-cm^{-1} peak. It is strongly enhanced by the 615-nm band, and it is enhanced as well by the 435-nm band, but it shows no intensity when excited in resonance with the intense 524-nm absorption band. The enhancement profiles of the peaks which do not shift upon isotopic substitution are shown in Figure 6. The 225- and 255-cm^{-1} peaks are both enhanced predominantly by the 615-nm band. The 333- and 650-cm^{-1} peaks each show intensity only to low energy, also indicating enhancement by the 615-nm band. Only the 430-cm^{-1} peak is enhanced predominantly by the intense 524-nm absorption band.

Analysis

A. Ground-State Vibrational Spectroscopy. The isotopic substitution of $^{16}O_2$ by $^{18}O_2$ in the preparation of $[\{Cu(TMPA)\}_2(O_2)]^{2+}$ shifts the vibrational frequencies of two peaks in its resonance Raman spectrum. The 44-cm^{-1} shift of the intense 832-cm^{-1} peak to 788 cm^{-1} in Figure 4 allows assignment of this feature as the oxygen–oxygen stretching frequency, ν(O–O). This is a typical intraligand stretching frequency for peroxide bound to transition metals, toward the high end of the range reported for a number of the analogous cobalt–peroxide dimers.[22] It is also consistent with the 1.432-Å O–O bond distance, typical for peroxide complexes, found in the X-ray crystal structure.[8] The 26-cm^{-1} shift of the 561-cm^{-1} peak to 535 cm^{-1} in Figure 4 indicates that it is a copper–oxygen stretch, ν(Cu–O). There are two copper–oxygen stretching modes expected in this dimer: the symmetric combination of the stretches of the two Cu–O bonds, which is of A_g symmetry, and the antisymmetric combination of B_u symmetry in the C_{2h} point group. The depolarization ratio of 0.4 indicates that the symmetric copper–oxygen stretch, ν_s(Cu–O), is observed as only totally symmetric Raman modes may have depolarization ratios less than 0.75. Due to the absence of observed isotope shifts, the remaining peaks in the metal–ligand region of the resonance Raman spectra must be associated with the non-peroxo ligands. The 650-cm^{-1} peak is too high in energy to be ν(Cu–N),[23] but it is in the correct energy region to be due to an internal mode of the coordinated pyridine rings.[24] The 430-cm^{-1} mode is too high in energy to be ν(Cu–N_{py}) from a pyridine nitrogen, which is generally observed to be lower than 270 cm^{-1}.[23] However, it is at a reasonable energy to be either ν(Cu–N_{ax}) due to the axial amine nitrogen coordinated to the copper opposite the peroxide or the lowest energy pyridine internal mode. Its much different enhancement behavior from the 650-cm^{-1} peak seems to indicate ν(Cu–N_{ax}) as the more likely assignment. The 333-cm^{-1} peak shows similar enhancement behavior to the 650-cm^{-1} peak but is too low in energy to be the lowest energy pyridine mode and too high in energy to be ν(Cu–N_{py}); it could be assigned as some other internal mode of the ligand system. The 225- and 255-cm^{-1} peaks show similar enhancement behavior and are at appropriate energies to be ν(Cu–N_{py}) modes from the coordinated pyridine nitrogens.

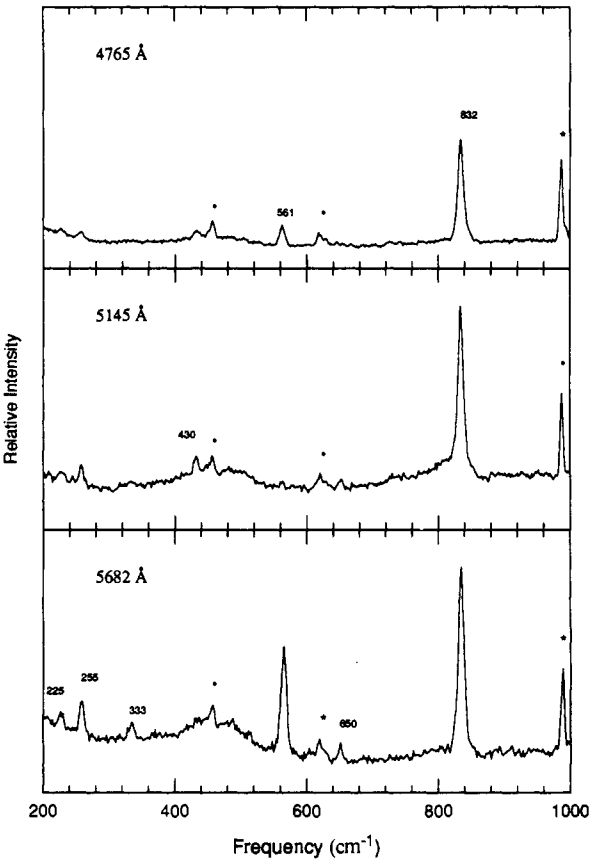

Figure 3. Resonance Raman spectra of solid $[\{Cu(TMPA)\}_2(O_2)](PF_6)_2$ dispersed in K_2SO_4 with excitation frequencies of 4765, 5145, and 5682 Å. Integration times were 5, 5, and 10 s, respectively. The 5145-Å spectrum is the sum of 2 scans, the others are 1 scan. Laser power was 60, 70, and 40 mW, respectively. Asterisks indicate SO_4^{2-} peaks.

A normal-coordinate analysis of the vibrational spectrum of the peroxide-bridged dimer, $[\{Cu(TMPA)\}_2(O_2)](PF_6)_2$, was undertaken for comparison to our vibrational studies on the terminally bound copper–peroxide monomer $[Cu_2(XYL\text{–}O\text{–})(O_2)]^+$ reported earlier.[4] The geometric parameters of the $[\{Cu(TMPA)\}_2(O_2)](PF_6)_2$ structure[8] (O–O bond distance, Cu–O bond distance, and Cu–O–O angle) were used to construct a terminally bound peroxide–copper monomer with structure A in Scheme I. The intraperoxide and copper–oxygen stretching force constants, $k_{O\text{–}O}$ and $k_{Cu\text{–}O}$, were fit to ν(O–O) and ν(Cu–O), the frequencies observed to correspond to the intraperoxide and copper–oxygen stretching modes in the Raman spectrum of $[Cu_2(XYL\text{–}O\text{–})(O_2)]^+$. Since no peak corresponding to the copper–peroxide bending mode, δ(Cu–O–O), was found in the vibrational spectrum of $[Cu_2(XYL\text{–}O\text{–})(O_2)]^+$ or $[\{Cu(TMPA)\}_2(O_2)](PF_6)_2$, a value of 174 cm^{-1}, which was

(22) Barraclough, C. G.; Lawrance, G. A.; Lay, P. A. *Inorg. Chem.* **1978**, *17*, 3317–3322.
(23) Adams, D. M. *Metal–Ligand and Related Vibrations*; St. Martin's Press: New York, 1968.
(24) Gill, N. S.; Nuttal, R. H.; Scaife, D. E.; Sharp, D. W. A. *J. Inorg. Nucl. Chem.* **1961**, *18*, 79–87.

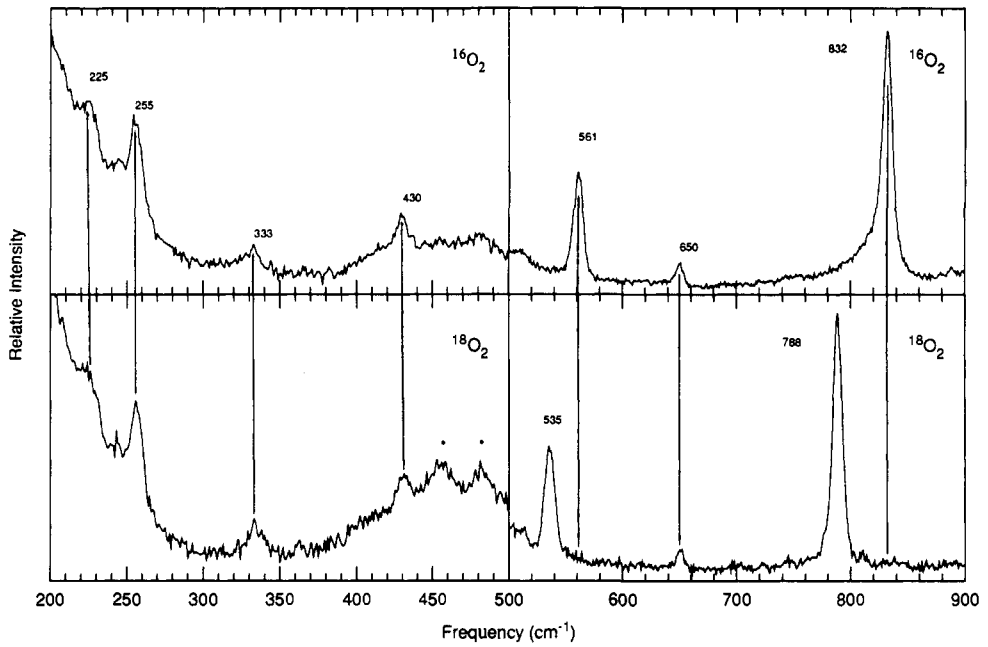

Figure 4. Resonance Raman spectra of solid $[\{Cu(TMPA)\}_2(O_2)](PF_6)_2$ made with $^{16}O_2$ and $^{18}O_2$, as indicated, dispersed in KBr. The spectra of the lower energy region are the sum of 40 scans with 5309-Å excitation. The higher energy region spectra are the sum of 10 scans with 5682-Å excitation. Integration time is 0.5 s and laser power is 60 mW.

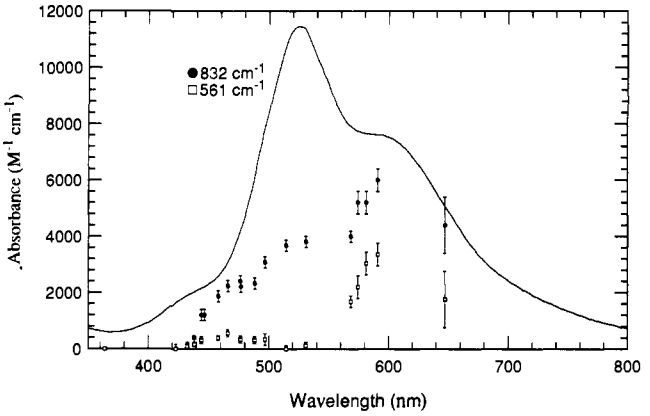

Figure 5. Resonance enhancement profiles of the 832- (●) and 561-cm^{-1} (□) Raman features of $[\{Cu(TMPA)\}_2(O_2)](PF_6)_2$. The optical absorption spectrum is also shown.

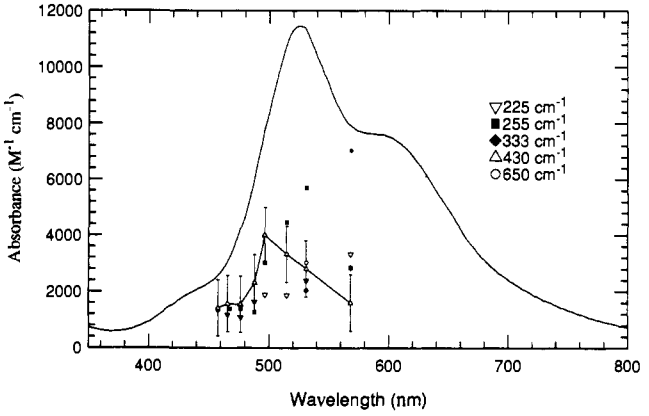

Figure 6. Resonance enhancement profiles of the Raman features of $[\{Cu(TMPA)\}_2(O_2)](PF_6)_2$ which do not shift upon isotopic oxygen substitution. The optical absorption spectrum is also shown.

observed and definitively assigned as δ_s(Co–O–O) in a cobalt–peroxide complex,[25] was used in the calculation. The intraperoxide force constant, k_{O-O}, is reasonably insensitive to the value chosen for δ(Cu–O–O). These monomer force constants, given in the top portion of the right-hand column of Table I, were then used to calculate ν(O–O) and ν(Cu–O) energies for the trans dimer geometry. It is seen from the values in Table I [in the columns labeled "calc(monomer fc's)"] that ν(O–O) is expected to increase from 799 to 809 cm^{-1} on going from the monomer to the dimer. This 10-cm^{-1} increase, which is due strictly to mechanical coupling effects, is much smaller than the observed 29-cm^{-1} increase from 803 to 832 cm^{-1}. This indicates that there is an increase in the O–O stretching force constant, k_{O-O}, on going from the monomer to the dimer complex. In addition, ν(Cu–O) is seen in the bottom portion of Table I to split into symmetric and antisymmetric components, with the symmetric component higher in energy. The energies of these components vary significantly depending on the value of δ_s(Cu–O–O) used in the calculation, and an accurate value of k_{Cu-O} cannot be obtained with an experimental value of only one of the four stretching or bending components. Since all our calculations using the same set of force constants for the monomer and the dimer result in lower bending frequencies in the dimer, and since too high a bending frequency results in reversal of the order of the symmetric and antisymmetric copper–peroxide stretching frequencies, a lower value of 140 cm^{-1} was used for δ_s(Cu–O–O) in the dimer calculation. The force constants thus obtained for the dimer are given in the bottom portion of the right-hand column of Table I.

The normal-coordinate calculations were extended to a planar cis μ-1,2 peroxide-bridged copper dimer, as in structure C in Scheme I. Using the force constants, the O–O and Cu–O bond lengths, and the Cu–O–O angle from $[\{Cu(TMPA)\}_2(O_2)](PF_6)_2$, the energy of ν(O–O) does not change significantly on going from the trans to the cis geometry. The energy ordering of ν_s(Cu–O) and ν_{as}(Cu–O) is opposite that of the trans geometry, placing the Raman-active symmetric mode lowest in energy at about 420 cm^{-1}. When the Cu–O–O angle is changed to allow for a 3.6-Å Cu–Cu distance as in oxyhemocyanin, an increase in the ν(O–O) energy of about 20 cm^{-1} is calculated. The calculations on the cis geometry do not take into account, however, the effects of a possible second bridging ligand such as hydroxide which would introduce additional mechanical coupling effects.

B. Excited-State Spectroscopy. While the full crystallographic symmetry of $[\{Cu(TMPA)\}_2(O_2)]^{2+}$ is C_i, the four-atom Cu_2O_2 unit (D in Scheme I) has C_{2h} symmetry which will be used to assign the charge-transfer spectrum. An ideal trigonal-bipyramidal ligand field would leave the d_{z^2} orbital on each Cu(II) half filled in the ground state. However, the ligand field in this complex is distorted from ideal trigonal-bipyramidal geometry which allows mixing of other d orbital character into the half-filled d_{z^2} orbital. On going to the dimer, each of the two $O_2^{2-}(\pi^*) \rightarrow Cu(d_{z^2})$ transitions in the monomer is energetically split into a singlet and a triplet excited state. Each singlet or triplet is further split into the symmetric and antisymmetric combinations of the transitions to each of the two coppers. In the C_{2h} dimer, the $\pi^*_\sigma \rightarrow$ Cu transitions are of $^{1,3}A_g$ and $^{1,3}B_u$ symmetry, while the $\pi^*_v \rightarrow$ Cu transitions are of $^{1,3}B_g$ and $^{1,3}A_u$ symmetry. For each set of four transitions, only the transitions to u

(25) Hester, R. E.; Nour, E. M. *J. Raman Spectrosc.* **1981**, *11*, 43–48.

components are electric dipole allowed and only the singlets are spin allowed. The bands at 524 and 615 nm in the absorption spectrum of the dimer may reasonably be assigned as the electric dipole allowed singlet components of the O_2^{2-} (π^*) → Cu(d_{z^2}) transitions, as they are significantly more intense than any other feature in this region and they show resonance enhancement of peroxide vibrational features. On the basis of their energy ordering and relative intensities, the higher energy and more intense band at 524 nm is assigned as the transition to the $^1B_u(\pi^*_\sigma)$ state, and the band at 615 nm is assigned as the transition to the $^1A_u(\pi^*_v)$ state. The 615-nm transition is somewhat more intense than expected for the π^*_v transition. It has about 35% of the intensity of the π^*_σ transition, as compared to 10% for the corresponding transitions in the $[Cu_2(XYL\text{-}O\text{-})(O_2)]^+$ monomer. This intensity must be inherent to the π^*_v transition as the resonance Raman profiles show significantly different enhancement of the vibrational features by the 524- and 615-nm transitions which indicates that there is not significant mixing of the π^*_σ and π^*_v wave functions. This increased intensity for the $O_2^{2-}(\pi_v^*) \rightarrow Cu(d_{z^2})$ transition likely derives from mixing of the half-occupied d_{z^2} orbital with other d orbitals with which the peroxide π^*_v orbital has significant overlap, due to the distortion from an idealized trigonal-bipyramidal geometry.

Significant differences in the excited-state distortions for these different peroxide-to-copper charge-transfer excited states have been found to be present from the resonance Raman enhancement profiles. The intensity of the enhanced Raman feature should be proportional to the square of the excited-state distortion along the corresponding normal mode, as well as the square of the oscillator strength of that resonant transition.[26] Since in the ground state the π^*_v peroxide orbital donates significantly less of its electron density into the copper–peroxide bond than does the π^*_σ orbital, it has more electron density with antibonding character in the intraperoxide region than does the π^*_σ orbital. Thus, the $\pi^*_v \rightarrow$ Cu transitions are expected to result in greater distortion of the O–O bond length and greater resonance enhancement of ν(O–O) relative to the square of their absorption intensities. Likewise, since the π^*_σ orbital is more bonding than π^*_v with respect to the copper–peroxide bond, ν(Cu–O) is expected to show greater resonance enhancement from the $\pi^*_\sigma \rightarrow$ Cu transitions. This type of resonance enhancement behavior was observed for $[Cu_2(XYL\text{-}O\text{-})(O_2)]^+$.[4a] The resonance enhancement profile of the 832-cm^{-1} ν(O–O) Raman peak in Figure 5 is consistent with the above assignment of the 524- and 615-nm absorption bands in $[\{Cu(TMPA)\}_2(O_2)]^{2+}$ as ^1B_u and ^1A_u, respectively. It is enhanced by both the $\pi^*_\sigma \rightarrow Cu(d_{z^2})$ (^1B_u) and the $\pi^*_v \rightarrow Cu(d_{z^2})$ (^1A_u) transitions, but more so by the transition from π^*_v. In contrast, the resonance enhancement profile of ν_s(Cu–O) in Figure 5 shows strong enhancement by the $\pi^*_v(^1A_u)$ transition but no enhancement by the $\pi^*_\sigma(^1B_u)$ transition, which is much different from the enhancement behavior seen for ν(Cu–O) in the $[Cu_2(XYL\text{-}O\text{-})(O_2)]^+$ monomer. However, the excited-state distortions along the Cu–O stretching mode are expected to be strongly affected upon going from a monomer to a dimer, resulting in significant changes in the enhancement behavior of the ν(Cu–O) Raman peak (see Discussion).

The enhancement profile of ν_s(Cu–O) indicates that the excited-state distortion associated with the 435-nm transition is similar to that of the 615-nm transition but not the 524-nm transition. The 435-nm transition is therefore assigned as a second component of the $\pi^*_v \rightarrow Cu(d_{z^2})$ transition. Since only the $\pi^*_v(^1A_u)$ and the $\pi^*_\sigma(^1B_u)$ transitions are fully allowed, the 435-nm band must be either the ^1B_g component of the π^*_v transition gaining intensity by vibronic coupling with ^1A_u through one of the two B_u vibrational modes or with ^1B_u through the A_u mode or the ^3A_u component of π^*_v gaining intensity by spin–orbit coupling with ^1A_u through the L_zS_z operator or with ^1B_u through L_xS_x or L_yS_y.

The energy shifts and splittings of the excited states on going from a monomer to a dimer[4b] are determined by four matrix elements as shown in Figure 7. The first is the electronic Coulomb integral, K, which causes all four components of a transition to shift equally. This contribution is expected to stabilize the peroxide π^* orbitals in the dimer due to the greater electron withdrawing ability of two copper ions as compared to one in the monomer. It should result in greater stabilization of π^*_σ due to its stronger bonding to the coppers than π^*_v, so that the average energy of each $\pi^* \rightarrow$ Cu(d) transition manifold should increase as should the difference in average energy between π^*_σ and π^*_v. The second contribution is the excited-state exchange integral, J_{es},[27] which results in splitting of the singlet and triplet excited states, where the singlet–triplet splitting is $-2J_{es}$. The final two contributions are the I and L integrals, the excitation-transfer terms mediated by Coulomb and exchange mechanisms, respectively. These terms transfer the peroxide-to-copper

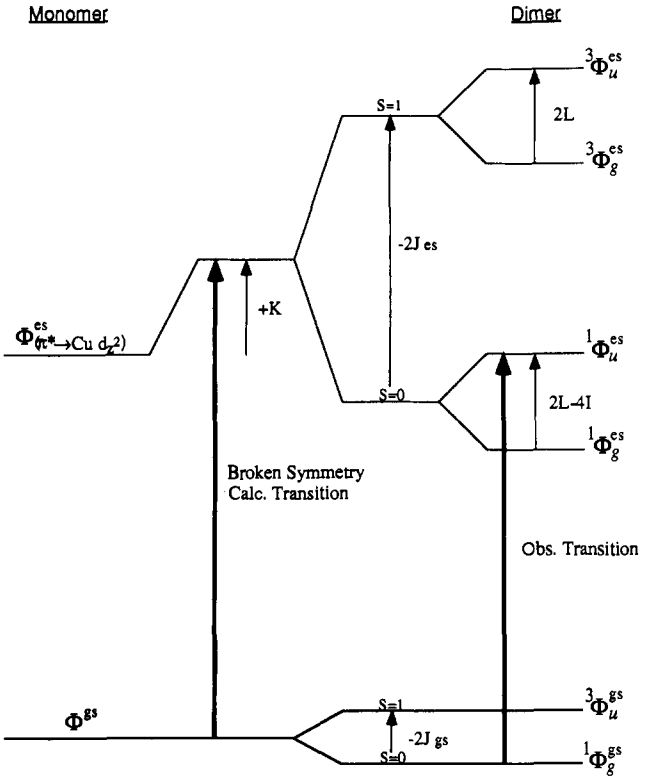

Figure 7. Energy level splitting diagram of the ground and excited states of a copper dimer. The calculated broken-symmetry transition and the observed spin and electric-dipole allowed transition are indicated by bold arrows.

charge-transfer transition from one side of the dimer to the other without (I) and with (L) electron transfer and are responsible for the splitting of the symmetric and antisymmetric combinations of the transitions. Together, these four terms lead to the energy expressions in eqs 1a–d for the dimer excited states relative to the monomer excited state as shown in the upper manifold of Figure 7.[28]

$$E(^1\Phi_g) = K_{\pi^*,d_{z^2}} + J_{\pi^*,d_{z^2}} + 2I_{\pi^*,d_{z^2}} - L_{\pi^*,d_{z^2}} \quad (1a)$$

$$E(^1\Phi_u) = K_{\pi^*,d_{z^2}} + J_{\pi^*,d_{z^2}} - 2I_{\pi^*,d_{z^2}} + L_{\pi^*,d_{z^2}} \quad (1b)$$

$$E(^3\Phi_g) = K_{\pi^*,d_{z^2}} - J_{\pi^*,d_{z^2}} - L_{\pi^*,d_{z^2}} \quad (1c)$$

$$E(^3\Phi_u) = K_{\pi^*,d_{z^2}} - J_{\pi^*,d_{z^2}} + L_{\pi^*,d_{z^2}} \quad (1d)$$

The contribution of the I integral to the g/u splitting of the singlet (ΔE_I(u–g) = $-4I$) may be estimated by a dipole–dipole approximation using the following equation:[29]

$$\Delta E_I(\text{u-g}) = \frac{2|\mathbf{M}|^2}{R^3}(1 - 3\cos^2\theta)$$

where $\mathbf{M}$ is the transition moment, R is the center-to-center distance between dipoles, and θ is the angle between each dipole and the dipole–dipole axis ($\theta = 0°$ for π^*_σ and 90° for π^*_v). On the basis of the transition moments of the 524- and 615-nm bands, values of $\Delta E(^1B_u\text{–}^1A_g) = -4I_\sigma = -21900\ cm^{-1}$ and $\Delta E_I(^1A_u\text{–}^1B_g) = -4I_v = +1700\ cm^{-1}$ were calculated for $\pi^*_\sigma \rightarrow Cu(d_{z^2})$ and $\pi^*_v \rightarrow Cu(d_{z^2})$, respectively.[30] The calculated g/u splitting of the $\pi^*_v \rightarrow Cu(d_{z^2})$ transition based only on

(26) Spiro, T. G.; Stein, P. *Annu. Rev. Phys. Chem.* **1977**, *28*, 501–521.
(27) The excited-state singlet–triplet splitting term is denoted as $-2J_{es}$. The ground-state singlet–triplet splitting is $-2J$.

(28) These expressions for charge-transfer transitions from a bridging ligand are different from those derived for the d–d transitions of the copper acetate dimer in ref 14 since the d–d transitions require a two-electron description while charge transfer from a bridging ligand requires a four-electron description. Figure 11 in ref 10b and Figure 15 in ref 15 use a two-electron description for charge transfer from a bridging ligand; however, this does not affect any of the conclusions in those papers. This will be discussed in a future study.[31]
(29) Kasha, M.; Rawls, H. R.; El-Bayoumi, M. A. *Pure Appl. Chem.* **1965**, *11*, 371–392.
(30) In order to take into account the localized (π^*_v) and delocalized (π^*_σ) nature of these transitions, as described in the Discussion section, the transition vector for the π^*_v transition was taken as the Cu–O bond, and for the π^*_σ transition from the center of the O–O bond to the copper. The transition moment, |M|, is in angstroms and is obtained from the oscillator strength, f, using the expression $|\mathbf{M}|^2 = [f/(2/\nu_0)](3h/8\pi^2 m_e)$.

Table II. Energy Levels and Charge Distributions (Copper Sphere Radius = 2.95 bohr)

	level	energy, eV	charge distribution[a] (%)							
			Cu1	Cu2	O1	O2	$N_{ax}1$	$N_{eq}1$	$N_{ax}2$	$N_{eq}2$
d_{z^2}	31A′↑	−6.536	3	67	2	8	0	0	6	9
	31A′↓	−6.536	67	3	8	2	6	9	0	0
d_{z^2}	30A′↑	−7.257	66	4	0	8	8	10	1	1
	30A′↓	−7.257	4	66	8	0	1	1	8	10
π^*_v	18A″↑	−7.890	6	40	16	24	0	1	0	5
	18A″↓	−7.890	40	6	24	16	0	5	0	1
	29A′↑	−8.288	0	84	0	0	0	0	0	9
	29A′↓	−8.288	84	0	0	0	0	9	0	0
	17A″↑	−8.409	6	71	7	4	0	1	0	5
	17A″↓	−8.409	71	6	4	7	0	5	0	1
	16A″↑	−8.882	53	30	3	1	0	9	0	0
	16A″↓	−8.882	30	53	1	3	0	0	0	9
	28A′↑	−8.943	39	50	1	1	0	6	0	0
	28A′↓	−8.943	50	39	1	1	0	0	0	6
	27A′↑	−8.998	44	45	0	1	0	6	0	0
	27A′↓	−8.998	45	44	1	0	0	0	0	6
	15A″↑	−9.263	55	26	10	2	0	2	0	0
	15A″↓	−9.263	26	55	2	10	0	0	0	2
	26A′↑	−9.754	92	1	2	1	0	0	0	0
	26A′↓	−9.754	1	92	1	2	0	0	0	0
	14A″↑	−10.134	57	15	6	17	0	0	0	0
	14A″↓	−10.134	15	57	17	6	0	0	0	0
π^*_σ	25A′↑	−10.722	13	13	28	33	6	0	6	0
	25A′↓	−10.722	13	13	33	28	6	0	6	0

[a] N_{ax} is the axial nitrogen, and N_{eq} is the sum of the equatorial nitrogens.

Coulomb interactions between transition moments predicts the ^1B_g transition to be at lower energy than ^1A_u. However, this does not take into account the contribution from the L term. An analysis of the physical origin of the L term shows that L must be positive if the transition is delocalized and relatively small if it is localized,[31] which also places ^1A_u at higher energy than ^1B_g. Therefore, the 435-nm absorption band cannot be the transition to the ^1B_g component of π^*_v and is assigned as the ^3A_u component of the π^*_v transition. From eqs 1 and the absorption spectrum in Figure 1, it is seen that $\Delta E(^3A_u - {}^1A_u) = -2J_{es} + 2I = 6750\ cm^{-1}$. Using the value of I_v calculated above, $-2J_{es} = 7600\ cm^{-1}$ for the π^*_v excited state. In the π^*_σ excited state a hole is created in this ligand orbital which has a very large overlap with a half-occupied d_{z^2} orbital on the second copper. Therefore, a large antiferromagnetic coupling is expected due to the large overlap of the orbitals containing the unpaired electrons. For the π^*_v excited state in rigorous C_{2h} symmetry with ideal trigonal-bipyramidal copper geometry, the orbitals with the unpaired spin density (Cu(II) d_{z^2} and O_2^{2-} π^*_v) would be orthogonal which would result in ferromagnetic coupling. However, the large amount of absorption intensity associated with the $\pi^*_v(^1A_u)$ transition at 615 nm indicates that these orbitals are not orthogonal (due to the distortion of each copper center away from trigonal-bipyramidal geometry) and have significant overlap, so that, as observed, antiferromagnetic coupling may be expected in this excited state as well.

The weak band observed at 1035 nm in Figure 2 may be assigned by comparison to other trigonal-bipyramidal copper complexes with similar ligands. Several complexes with one axial and three equatorial amine nitrogen ligands and an axial ammonia or halide have two low-energy features, the more intense of which occurs between 9500 and 11 500 cm^{-1} with the second feature appearing as a shoulder to higher energy between 13 000 and 15 200 cm^{-1}.[32] These features have been assigned as the $d_{xy,x^2-y^2} \rightarrow d_{z^2}$ and $d_{xz,yz} \rightarrow d_{z^2}$ transitions, respectively. The chloride analogue, $[Cu(TMPA)Cl]^+$, fits this description with an absorption band at 10 500 cm^{-1} and a shoulder at 13 200 cm^{-1}. By analogy, the band at 9660 cm^{-1} in the peroxide complex may be assigned as the $d_{xy,x^2-y^2} \rightarrow d_{z^2}$ transition, while the $d_{xz,yz} \rightarrow d_{z^2}$ transition is obscured by the intense low-energy tail of the charge-transfer transitions. The d–d transitions should also split due to dimer interactions; however, this splitting is expected to be small[14] compared to that in the charge-transfer transitions.

C. Broken-Symmetry SCF-Xα-SW Calculations. Spin-unrestricted, broken-symmetry SCF-Xα-SW calculations were performed on $[(NH_3)_4CuO_2Cu(NH_3)_4]^{2+}$ with an idealized trigonal-bipyramidal coordination environment for each of the two cupric ions, which are bridged by peroxide in a trans μ-1,2 geometry. The bonding is qualitatively similar to that described in greater detail for complex **2** in ref 10b, except that in this case the unpaired electrons are in the d_{z^2} orbital of each copper due to the trigonal-bipyramidal rather than square-planar ligand field. Due to the nature of the broken-symmetry state, in which the full molecular symmetry of C_{2h} is lowered to C_s and an equal but opposite up–down spin symmetry is imposed on the two halves of the dimer, the energy levels may be partially localized onto one-half of the molecule. Each spin-up electron is energetically degenerate with a spin-down electron on the opposite side of the molecule, such that spin-up and spin-down one-electron orbitals are images of one another under inversion. The extent of localization is indicated by the charge distributions presented in Table II. For example, the π^*_v level 18″↑ has 6% of the electron density on Cu1 and 16% on O1, but 40% and 24% on Cu2 and O2, respectively. In contrast, the π^*_σ level 25A′↑ has its electron density distributed nearly equally over the two halves of the dimer. Both levels 31A′↓ (LUMO) and 30A′↑ (HOMO) are localized on Cu1 and have strong antibonding interactions with the nitrogen and peroxide ligands which cause them to be higher in energy than the other Cu d orbitals. In addition, the positive linear combination of Cu d_{z^2} orbitals in level 31A′↓ has an antibonding interaction between the peroxide and Cu2, which causes it to be higher in energy than the negative linear combination of Cu d_{z^2} orbitals in level 30A′↑, which has a weak bonding interaction between the peroxide and Cu2. Thus, spin polarization in the broken-symmetry state causes a large splitting between the spin-up and spin-down d orbitals on a given copper, as seen for the splitting of levels 30A′↑ and 31A′↓ in Table II. The electron density contours for levels 30A′↑ and 31A′↓ are similar to those in Figure 5, B and A, respectively, in ref 10b. Levels 30A′↓ and 31A′↑ are the energetically degenerate inversion images located on Cu2.

The HOMO–LUMO energy difference is related to the antiferromagnetic properties of the ground state since the singlet ground state has 30A′↑ and 30A′↓ both occupied and 31A′↑ and 31A′↓ unoccupied while the lowest energy triplet state requires occupation of the like-spin one-electron orbitals of levels 30A′ and 31A′. The broken-symmetry formalism was specifically developed to treat the interactions between antiferromagnetically coupled transition-metal ions, and one of the advantages of this formalism is the ability to use projection operator techniques to determine the sign and magnitude of the ground-state superexchange interactions.[33] For weakly interacting copper dimers, the ground-state singlet–triplet splitting, $-2J$ ($H = -2J(\mathbf{S}_i\mathbf{S}_j)$), can be directly calculated by the Slater transition-state method.[34] By converging to a transition state in which half an electron is moved from the 30A′↑ level to the 31A′↓ level, the singlet–triplet splitting is twice the energy difference between the two levels.[33] The resulting calculated value of 500 cm^{-1} for the ground-state singlet–triplet splitting is reasonably consistent with the experimental value ($-2J \geq 600\ cm^{-1}$)[11] for $[\{Cu(TMPA)\}_2(O_2)]^{2+}$. This value represents a moderately large antiferromagnetic superexchange interaction, which is transmitted solely through the peroxide bridge.

As indicated by the charge distribution in Table II, the highest energy level with significant electron density on the oxygen atoms is 18A″. It is composed primarily of the peroxide π^*_v orbital, which is out of the copper–peroxide plane, and interacts weakly with the Cu $d_{xy,yz}$ orbitals and through these with the equatorial nitrogen ligands. Level 25A′, which is also localized on the oxygen atoms, lies below the filled Cu d orbitals. It is composed primarily of the in-plane peroxide π^*_σ orbital and includes a strong, stabilizing σ-bonding interaction with the symmetric combination of half-occupied Cu(d_{z^2}) orbitals and a weak interaction with the axial nitrogen ligand. The electron density contour of this level is similar to that in Figure 5C of ref 10b. This bonding interaction between the Cu d_{z^2} and peroxide π^*_σ orbitals is the dominant contribution to the copper–peroxide bond and lowers the energy of the π^*_σ level (25A′) well below that of the π^*_v level (18A″), leading to the large $\pi^*_v - \pi^*_\sigma$ splitting of 2.832 eV indicated in Table II. Calculations

Table III. Calculated Spin-Allowed Excited-State Transition Energies[a]

Cu radius	18A″↑(π^*_v)	25A′↑(π^*_σ)	lowest ↑ d–d	highest ↑ d–d
2.33	14 200	28 700	19 800	32 500
2.60	13 200	35 200	19 600	27 500
2.95	11 900	40 500	16 100	21 800
exp[b]	16 250	19 100	9660	

[a] The transitions are one-electron excitations from the indicated level to the 31A′↑ level in units of cm^{-1}. [b] The experimental values are for $[\{Cu(TMPA)\}_2(O_2)]^{2+}$.

(31) Tuczek, F.; Solomon, E. I. Manuscript in preparation.
(32) Duggan, M.; Ray, N.; Hathaway, B.; Tomlinson, G.; Brint, P.; Pelin, K. *J. Chem. Soc., Dalton Trans.* **1980**, 1342–1348.
(33) (a) Noodleman, L.; Norman, J. G., Jr. *J. Chem. Phys.* **1979**, *70*, 4903–4906. (b) Noodleman, L. *Ibid.* **1981**, *74*, 5737–5743.
(34) Slater, J. C. *The Self-Consistent Field for Molecules and Solids; Quantum Theory of Molecules and Solids*; McGraw-Hill: New York, 1974; Vol. 4.

with Norman sphere radii and with copper sphere radii of 2.60 bohr are qualitatively similar (supplementary material, Table SII).

The calculated excited-state transition energies for the π^*_v and π^*_σ charge-transfer transitions, and for the lowest and highest energy ligand-field transitions, are presented in Table III. Several important trends can be seen. First, as the copper sphere radii are increased, the d–d transitions decrease in energy, but do not become as low as those observed experimentally. Second, the lowest energy transition is calculated to be the $\pi^*_v \rightarrow$ Cu charge-transfer transition, in agreement with the lowest observed charge-transfer transition being assigned as the allowed singlet component (^1A_u) of that transition. Third, the calculated transition energies, especially for π^*_σ, are very dependent on the copper sphere radii as a direct result of changes in the calculated covalency of the metal–ligand interactions.[10b]

The dependence of the calculated transition energies on the copper sphere radii is not the only contribution to the discrepancy between the observed and calculated transition energies. Transition energies calculated in the broken-symmetry formalism do not directly correspond to the transition energies that are experimentally observed in the absorption spectrum. As presented in section B of the Analysis and shown in Figure 7, each monomer-like excited-state transition splits into four components in the dimer. Each experimentally observed transition corresponds to one of these four components of an excited state ($^1\Phi_u^{es}$) as indicated by the bold arrow on the right side of Figure 7. However, because the broken-symmetry formalism is based on a single-determinant method, the calculated transition energy from the broken-symmetry ground state to the mixed-spin, mixed-symmetry excited state corresponds to an average of the excited state components as indicated by the bold arrow on the left side of Figure 7. Although the SCF-Xα-SW calculated transition energy includes the K term from eq 1b, the remaining terms contribute to the observed energy but not the calculated energy, so that $(E_{exp} - E_{calc}) = J_{es} + L - 2I$. For the π^*_v transition, $J_{es} = -3800$ cm^{-1} and $-2I = 850$ cm^{-1} from section B of the Analysis. Although the magnitude of L is not experimentally observed, L relates to direct excitation exchange between the two copper centers, so its magnitude is highly dependent upon the extent of coupling between the two sides of the dimer. Thus, for the π^*_v case which the charge distributions in Table II show to be very localized, L can be assumed to be small. The magnitudes of these three components in the splitting of the π^*_σ transition are all much larger than those for the π^*_v transition. The magnitude of J_{es} is dependent upon the overlap between the orbitals containing the unpaired electrons, and since this overlap is indicated by the relative charge-transfer intensities to be much greater for π^*_σ than for π^*_v, J_{es} will also be at least several times larger for π^*_σ than for π^*_v. From section B of the Analysis, $-2I = -10950$ cm^{-1} for π^*_σ, and due to its delocalization indicated by the charge distributions in Table II, L may be expected to be large as well. The greater magnitude of the J_{es}, I, and L terms for π^*_σ results in a larger discrepancy between the observed and calculated values for the π^*_σ transition than for the π^*_v transition, as seen in Table III.

Discussion

A general bonding description of the end-on bound peroxide-bridged copper dimer complex has been obtained from the broken-symmetry SCF-Xα-SW calculations. Electron donation into the half-occupied Cu d_{z^2} orbitals from the σ-bonding component of the pair of peroxide π^* orbitals provides the primary bonding interaction. This interaction causes a large energy stabilization of this π^*_σ level compared to the π^*_v level, which has less overlap with the half-occupied orbital on the copper. This is responsible for the general energy splitting and intensity pattern of the $\pi^*_v/\pi^*_\sigma \rightarrow$ Cu(II) charge-transfer transitions in the absorption spectrum. Dimer interactions further split the excited states resulting from charge-transfer transitions from these π^* orbitals to the coppers into four components which are averaged in the broken-symmetry calculations. Therefore, the calculated transition energies in Table III correspond to the average of the four components; since these splittings should be larger for the π^*_σ excited state, its observed transition energy deviates from the calculated value by more than the π^*_v transition energy. In addition, it is found from the calculated charge distributions in Table II that the one-electron spin orbitals that compose the π^*_σ (25A′) are delocalized over both sides of the dimer. In contrast, the one-electron orbitals of the π^*_v (18A″) are each localized on one side of the dimer. In the delocalized case (π^*_σ), excitation of an electron into the half-occuped copper d_{z^2} orbitals results in an excited state in which the two sides of the dimer are strongly coupled while in the localized case (π^*_v) the excitation results in an excited state in which the two sides of the dimer are weakly coupled. This has significant consequences with respect to excited-state distortions associated with these transitions (vide infra). The HOMO and LUMO orbitals in the ground state consist of the spin up/down pairs of the negative and positive linear combinatins of the Cu(d_{z^2}) orbitals, respectively. The ground-state antiferromagnetic singlet–triplet splitting is determined by the energy difference between these two orbitals, which results from the stronger antibonding interaction of the LUMO with the π^*_σ orbital.

The Raman study provides important new insight into the ground-state vibrational and electronic structure of the trans μ-1,2 peroxo-bridged copper dimer $[\{Cu(TMPA)\}_2(O_2)]^{2+}$ when compared to our previous study of the copper peroxide monomer $[Cu_2(XYL-O-)(O_2)]^+$. The Raman peaks corresponding to ν(O–O) and ν_s(Cu–O) are definitely assigned in $[\{Cu(TMPA)\}_2(O_2)]^{2+}$ and are both seen to be higher in energy than the corresponding peaks in $[Cu_2(XYL-O-)(O_2)]^+$. The normal-coordinate analysis in Table I predicts that ν(O–O) will increase in energy due to mechanical interactions on going to the dimer, but not by nearly as much as observed. This requires that there is an increase in the O–O force constant, k_{O-O}. This increase in k_{O-O}, corresponding to an increased O–O bond strength, occurs because the second copper accepts additional electron density from the peroxide. This electron density is donated from the antibonding π^*_σ orbital of peroxide, thus effectively increasing the O–O bond order. The significant increase in the energy of the observed ν(Cu–O) peak from 488 to 561 cm^{-1} is due to its splitting into symmetric and antisymmetric components in the dimer. The normal-coordinate analysis indicates that the Raman-active, symmetric component should be the higher energy component in the end-on trans geometry. In the end-on cis geometry, the symmetric copper–oxygen stretch is predicted to be at lower energy than the antisymmetric stretch. In addition, in the cis geometry ν(O–O) is predicted to be at higher energy than for the trans geometry with the same force constants, rather than significantly lower as observed for oxyhemocyanin and oxytyrosinase.

In the absorption spectrum of $[\{Cu(TMPA)\}_2(O_2)]^{2+}$ we have identified four excited-state transitions. The lowest energy transition is the $d_{xy,x^2-y^2} \rightarrow d_{z^2}$ ligand field transition at an energy comparable to the corresponding transition in other trigonal-bipyramidal complexes with similar ligands.[32] The other three are peroxide (π^*)-to-copper (d_{z^2}) charge-transfer transitions with the two most intense being the fully allowed transitions from each π^* orbital. The total intensity of these charge-transfer transitions is about twice that observed for the corresponding transitions in the monomer consistent with the increased overlap of peroxide with the half-occupied d orbitals on two coppers in the dimer. The relative intensities of the individual bands are somewhat different, however. The larger than expected intensity of the allowed π^*_v transition in the dimer, which is the lowest energy Gaussian band in Figure 1, is accounted for by the deviation of the ligand field from ideal trigonal-bipyramidal geometry, allowing mixing of the d orbitals so that the overlap between π^*_v and the orbital with the unpaired electron density increases. Further, as indicated by the resonance Raman enhancement profiles in Figure 5, two components of the π^*_v transition manifold are observed: the allowed ^1A_u and spin-forbidden ^3A_u transitions. Spin–orbit coupling of the $^3A_u(\pi^*_v)$ transition with one of the allowed transitions (^1B_u or ^1A_u) gives this transition its absorption intensity. The observation and identification of this band allows us to explicitly obtain a singlet–triplet splitting for a charge-transfer excited state in a copper–peroxide complex for the first time. The value obtained, $-2J_{es} = 7600$ cm^{-1}, is an order of magnitude larger than the ground-state splitting. This is consistent with our studies on a chlorocuprate dimer,[35] which suggested a lower limit for the excited-state antiferromagnetic splitting which was also an order of magnitude larger than the ground-state splitting. This much larger singlet–triplet splitting in the excited state than in the ground state indicates a much better magnetic exchange pathway in the

(35) Desjardins, S. R.; Wilcox, D. E.; Musselman, R. L.; Solomon, E. I. *Inorg. Chem.* **1987**, *26*, 288–300.

charge-transfer excited state. In the ground state, the exchange occurs between the unpaired electrons on the two copper centers through the peroxide bridge acting as a superexchange pathway. In the π^*_v charge-transfer excited state, one unpaired electron remains in a d orbital on a copper but the other is in the peroxide π^*_v orbital. These orbitals have direct overlap which results in a much larger antiferromagnetic coupling of the unpaired electrons.

The various Raman peaks observed for this complex exhibit distinctively different resonance enhancement behavior, allowing insight into the excited-state distortions of the dimer. The intraperoxide stretch, ν(O–O), has enhancement behavior similar to that of the monomer. This indicates that the presence of a second copper does not significantly alter the excited-state distortion along this coordinate caused by the transition from either π^*_σ or π^*_v. However, this is not the case for the copper–oxygen stretch, ν(Cu–O), as can be seen by its strikingly different enhancement behavior in the dimer from that in the monomer. While the copper–oxygen stretch is strongly enhanced by the π^*_v transition, this vibration has virtually no intensity in resonance with the π^*_σ transition. This is contrary to the expected trend that greater distortion along the copper–oxygen bonds would result from a π^*_σ transition than from a π^*_v transition as the former involves removal of an electron from a copper–peroxide σ-bonding orbital. This apparently anomalous enhancement behavior of the copper–oxygen stretch in resonance with the π^*_σ transition must be due to effects in the dimer which do not occur in the monomer.

As discussed earlier in this section, the transition from π^*_v results in a weakly coupled excited state, while the transition from π^*_σ results in a strongly coupled excited state. The weak (eq 2a) and strong (eq 2b) coupling wave functions may be expressed as follows:[36,37]

$$\Psi_{weak} = 2^{-1/2}[\psi_1^{g}\varphi_1^{g0}\psi_2^{e}\varphi_2^{ei} \pm \psi_1^{e}\varphi_1^{ei}\psi_2^{g}\varphi_2^{g0}] \quad (2a)$$

$$\Psi_{strong} = 2^{-1/2}[\psi_1^{g}\psi_2^{e} \pm \psi_1^{e}\psi_2^{g}][\varphi_1^{ej}\varphi_2^{ej}] \quad (2b)$$

where, for example, ψ_1^g is the electronic part of the wave function of side 1 of the dimer in the ground state and φ_1^{ei} is the vibrational part of the wave function corresponding to a nuclear distortion on side 1 of the dimer due to the transition to electronic excited state e and vibrational state i of that electronic excited state. Expression 2a indicates that in the weak coupling case the excited-state wave function has two weakly interacting terms due to excitation on each side of the dimer with the resulting nuclear distortion being associated with the side of the dimer experiencing the excitation. Expression 2b indicates that the strong coupling case involves positive and negative combinations of the electronic excitation and nuclear distortions on both sides of the dimer. In a time-dependent approach,[36] this is equivalent to saying that in the weak coupling case, the excitation transfer is sufficiently slow that the nuclear distortion may "follow" the electronic excitation. In the strongly coupled case, there is sufficiently rapid excitation transfer that the nuclear distortion cannot accompany the electronic excitation and equal nuclear distortions occur on both sides of the dimer. The weakly coupled π^*_v transition in the dimer is similar to the π^*_v transition in the monomer, resulting in a monomer-like excited-state distortion and enhancement of the copper–oxygen stretching mode, as seen in Figure 5. In contrast, the excitation in the strongly coupled π^*_σ transition is delocalized over the two copper centers and is therefore significantly different from the π^*_σ transition in the monomer. The distorting forces along the copper–oxygen bonds are still expected to be greater for the transition from π^*_σ than from π^*_v. However, for the π^*_σ transition, these forces will be approximately equal and in opposing directions. Since the copper ions are held in place by their large ligand systems and correspondingly large effective mass, significant cancellation of forces will ensue and little distortion along the copper–oxygen stretching mode will occur. In the O–O stretching mode, however, only a single stretch is involved and no cancellation of forces occurs so that there is no effect due to delocalization.

The Raman peaks which are not related to peroxide also have interesting enhancement behavior in resonance with the peroxide-to-copper charge-transfer bands. The 430-cm^{-1} peak, which we have assigned as ν(Cu–N_{ax}), is enhanced by the π^*_σ transition but not significantly by the π^*_v transition (see the data points joined by the solid line in Figure 6). This is consistent with the charge distribution from the Xα calculations in Table II, which indicate that this axial copper–nitrogen bond contributes significantly to the π^*_σ orbital, but not to the π^*_v orbital. In contrast, two of the equatorial nitrogen ligands interact with π^*_v but not π^*_σ, consistent with the assignment of the 225- and 255-cm^{-1} Raman peaks as ν(Cu–N_{py}). In the resonance Raman spectra of oxyhemocyanin, enhancement of modes assigned as ν(Cu–N) has also been observed in resonance with peroxide-to-copper charge-transfer transitions.[38]

In this study, absorption and resonance Raman data and broken-symmetry SCF–Xα–SW calculations have been used to elucidate the vibrational and electronic structure and bonding of a structurally characterized end-on peroxide-bridged copper dimer. Significant effects on the ground-state vibrational structure and the charge-transfer excited states are seen on going from the monomer to the dimer. First, the normal-coordinate analysis of the vibrational spectrum shows that the O–O bond strength increases when a second copper is added due to increased donation of antibonding electron density from the intraperoxide region. Second, the splitting of the excited-state transitions in the dimer causes the observation of these transitions at significantly different energies than predicted by the broken-symmetry SCF–Xα–SW calculations. Third, the charge-transfer excited-state antiferromagnetic singlet–triplet splitting is found to be an order of magnitude greater than the ground-state singlet–triplet splitting due to direct overlap of the magnetic orbitals involved in the excited state. Finally, transitions in the dimer may be either delocalized or localized depending on whether the donor orbital strongly or weakly couples the two sides of the dimer. The degree of delocalization strongly influences the excited-state distortions as well as the magnitude of the g/u splittings of the excited states. The lack of resonance enhancement of the copper–oxygen vibration by the delocalized π^*_σ excited state appears to provide an explanation for the lack of an observed copper–oxygen stretching mode in the resonance Raman spectra of oxyhemocyanin[38] as well.

Acknowledgment. The authors thank Dr. Felix Tuczek for helpful discussions regarding charge-transfer excited-state splittings and Richard R. Jacobson for help in preparing the complexes used in this study. This research is supported by National Institute of Health Grants DK 31450 (E.I.S.) and GM 28962 (K.D.K.).

Supplementary Material Available: Atomic positions, energies, and charge decompositions for the one-electron eigenfunctions from SCF–Xα–SW calculations on $[(NH_3)_4CuO_2Cu(NH_3)_4]^{2+}$ with the Norman sphere radii, with the copper sphere radius equal to 2.60 bohr, and with the copper sphere radius equal to 2.95 bohr (16 pages). Ordering information is given on any current masthead page.

(36) Simpson, W. T.; Peterson, D. L. *J. Chem. Phys.* **1957**, *26*, 588–593.
(37) McClure, D. S. *Can. J. Chem.* **1958**, *36*, 59–71.
(38) Larrabee, J. A.; Spiro, T. G. *J. Am. Chem. Soc.* **1980**, *102*, 4217–4223.